Hindawi
Advances in Materials Science and Engineering
Volume 2018, Article ID 1416942, 9 pages
https://doi.org/10.1155/2018/1416942

*Research Article*

# Comparison of Sn-5Sb and Sn-10Sb Alloys in Tensile and Fatigue Properties Using Miniature Size Specimens

**Tatsuya Kobayashi, Kyosuke Kobayashi, Kohei Mitsui, and Ikuo Shohji**

*Graduate School of Science and Technology, Gunma University, 1-5-1 Tenjin-cho, Kiryu 376-8515, Japan*

Correspondence should be addressed to Tatsuya Kobayashi; t172b601@gunma-u.ac.jp

Received 26 December 2017; Revised 11 April 2018; Accepted 14 May 2018; Published 13 June 2018

Academic Editor: Marek Smaga



Tensile and low cycle fatigue properties of Sn-5Sb (mass%) and Sn-10Sb (mass%) were investigated using miniature size specimens, and fracture behaviors of the specimens were observed. Tensile strength and 0.1% proof stress of both alloys decrease with increasing the temperature. The tensile strength and 0.1% proof stress of Sn-10Sb are higher than those of Sn-5Sb at 25°C. Elongation of Sn-5Sb decreases with increasing the temperature except for a strain rate of $2 \times 10^{-1}$ s$^{-1}$, while Sn-10Sb increases with increasing temperature. Although elongation of Sn-10Sb is lower than that of Sn-5Sb at 25°C, the difference between them is small at 150°C. Chisel-point fracture was observed in both alloys regardless of conditions of the tensile test. The low cycle fatigue lives of Sn-5Sb and Sn-10Sb alloys obey the Manson–Coffin equation, and the fatigue ductility exponent, $\alpha$, was 0.54 for Sn-5Sb and 0.46 for Sn-10Sb in the temperature range from 25°C to 150°C. On the basis of the observation of fractured specimens and the investigation of $\alpha$, it was clarified that the crack progress can be delayed by the formation of coarse SbSn compounds in the Sn-Sb alloy, and thus the fatigue properties can be improved.

## 1. Introduction

Due to environmental regulations such as the Restriction of Hazardous Substances (RoHS) directive, lead-free soldering has spread to the world. Lead-free solder is classified broadly into three types depending on the temperature range: high-temperature solder [1–3], medium-temperature solder [3], and low-temperature solder [3, 4]. In general, high-temperature lead-free solder has been used for power semiconductor devices as a die-attach material. Pb-rich solder containing from 5 to 10 mass% Sn has been used for such applications. However, lead-free high-temperature solder alloys have not been regulated by RoHS directive yet, and such solders are expected to be developed [1, 5–8]. These solders need to be equipped with a combination of good mechanical properties, high thermal fatigue properties, and high heat resistance.

Sn-Sb alloys are one of the candidates for the substitution of the Pb-rich solders [9–11]. It has been reported that Sn-5Sb (mass%) has excellent thermal fatigue behaviors and relatively high fracture strength [12, 13]. In addition, in Sn-Sb alloys with high concentration of Sb, mechanical strength is improved by solid-solution of Sb in β-Sn matrix and dispersion of SbSn compounds [14].

The aim of this study is to compare tensile and low cycle fatigue properties of the Sn-5Sb (mass%) and Sn-10Sb (mass%) alloys using miniature size specimens, which have microstructures similar to real solder joints [15, 16]. Moreover, fracture behaviors of the specimens after tensile and fatigue tests were investigated.

## 2. Materials and Methods

*2.1. Specimen Preparation.* Ingots of Sn-5Sb and Sn-10Sb alloys were prepared. Melting properties of both alloys were investigated by differential scanning calorimetry (DSC). When the DSC was measured, the weight of the specimen was adjusted around 10 mg. The measurement was conducted at a heating rate of 10°C/min in the temperature range from 30°C to 300°C. From the DSC measurement

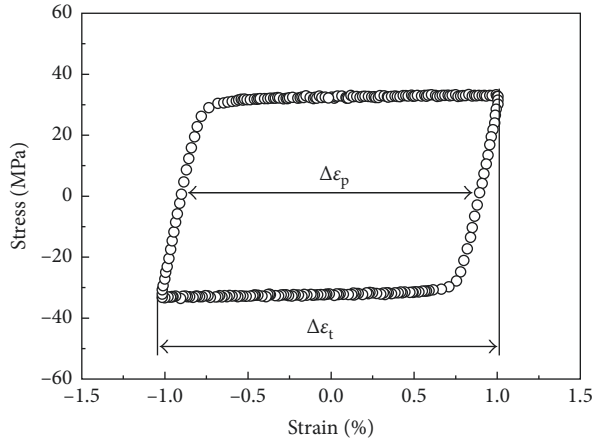


Figure 1: Example of stress-strain hysteresis loop at the tenth cycle in fatigue test (Sn-5Sb, $\Delta\varepsilon_t$: 2.0%, 25°C).

result, the solidus temperature and the melting finish temperature of the alloys were estimated to be 240°C and 248°C for Sn-5Sb and 248°C and 254°C for Sn-10Sb, respectively. Solder wire with 1.2 mm diameter was fabricated by drawing the ingot. As-cast miniature size specimens with $2.0 \pm 0.2$ mm gage length and $0.50 \pm 0.05$ mm diameter were fabricated from solder wire by casting [15]. A divided metal mold made of the 2219 aluminum alloy was prepared. The metal mold with solder wire was heated from 20°C to casting temperature. Casting was conducted at the temperature that is 10°C higher than the melting finish temperature. The maximum cooling rates in casting that were measured with a thermocouple put in the metal mold were 3.5°C/s and 3.6°C/s for Sn-5Sb and Sn-10Sb, respectively. In this study, as-cast miniature size specimens were used for the tensile test and the low cycle fatigue test.

*2.2. Microstructural Observation.* To observe microstructures of as-cast miniature size specimens, specimens were embedded in epoxy resin and cross sections were made perpendicular to the longitudinal direction. Afterwards, the cross sections were polished with #500–#4000 SiC papers and 1 $\mu$m alumina powder suspension. After polishing, the microstructural observation for the cross section of the specimen was conducted using a laser microscope and an electron probe X-ray microanalyzer (EPMA).

*2.3. Tensile Test.* Tensile tests were conducted at strain rates ranging from $2 \times 10^{-3}\,s^{-1}$ to $2 \times 10^{-1}\,s^{-1}$ at 25°C and 150°C. The test was conducted with a micro load test system (Saginomiya Seisakusho LMH207-10). In the test system, a linear servo motor that has an air-bearing system was used for an actuator to avoid mechanical contact. A linear encoder was used for a displacement detector, and the displacement resolution of the detector was within $\pm 0.1$ $\mu$m. Five specimens were tested under each condition. After the test, appearances and fracture surfaces of specimens were observed with the EPMA.

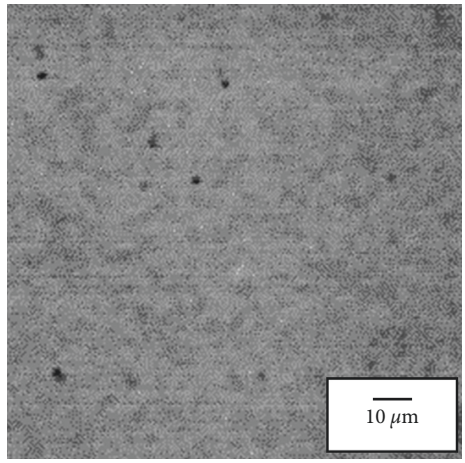


Figure 2: Back-scattered electron image of Sn-5Sb.

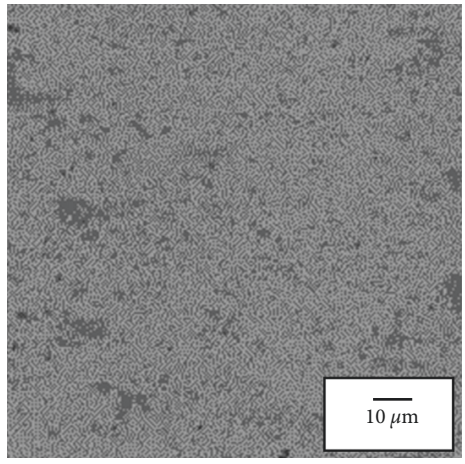


Figure 3: Back-scattered electron image of Sn-10Sb.

*2.4. Low Cycle Fatigue Test.* A low cycle fatigue test was also conducted with the micro load test system. The test was conducted at a strain rate of $2 \times 10^{-3}\,s^{-1}$ at 25°C and 150°C. In the test, strain was controlled using a symmetrical triangle wave, and the total strain range, $\Delta\varepsilon_t$, was controlled in the range of 0.4% to 2.0%. Figure 1 shows an example of the stress-strain hysteresis loop at the tenth cycle in the fatigue test. The inelastic strain range, $\Delta\varepsilon_p$, was defined as shown in Figure 1. The fatigue life was defined as the number of cycles in which the maximum load reduced by 20%. After the test, appearances and fracture surfaces of specimens were observed by the laser microscope and the EPMA. Moreover, the surface roughness of the fracture surfaces of the specimens were tested at the total strain range of 0.8% and 2.0%, which were measured at 20 fields by using a laser microscope, and then the average of maximum height, $R_z$, was calculated.

## 3. Results and Discussion

*3.1. Microstructure of Miniature Size Specimen.* Figures 2 and 3 show back-scattered electron (BSE) images of as-cast miniature size specimens of Sn-5Sb and Sn-10Sb, respectively.

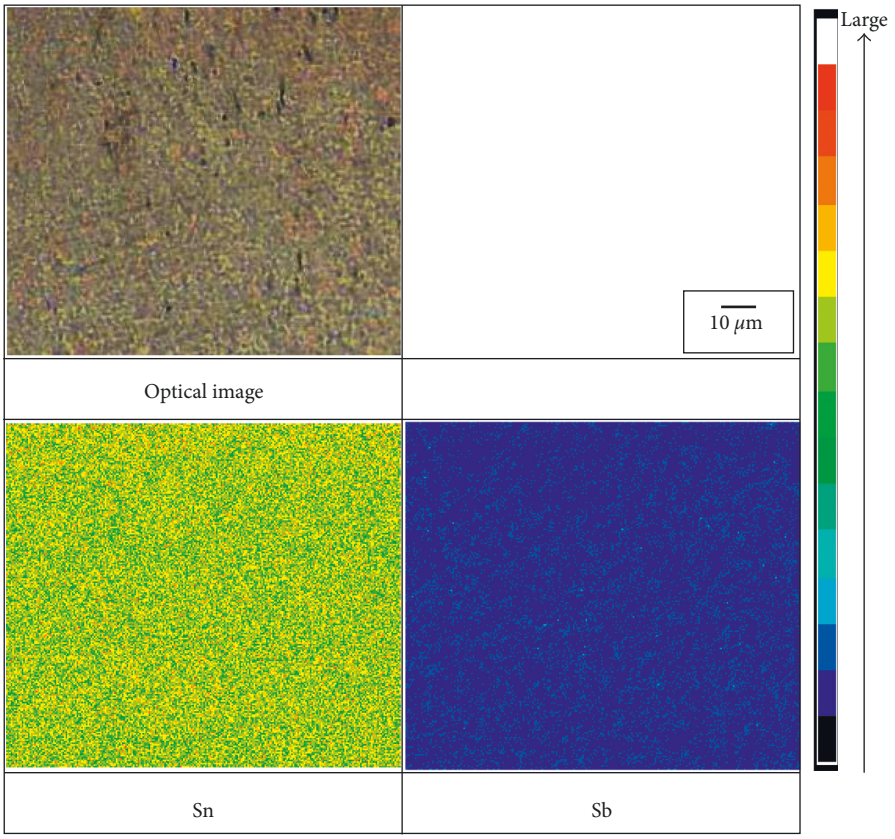


Figure 4: Laser scanning microscope image of Sn-5Sb and corresponding EPMA composition maps.

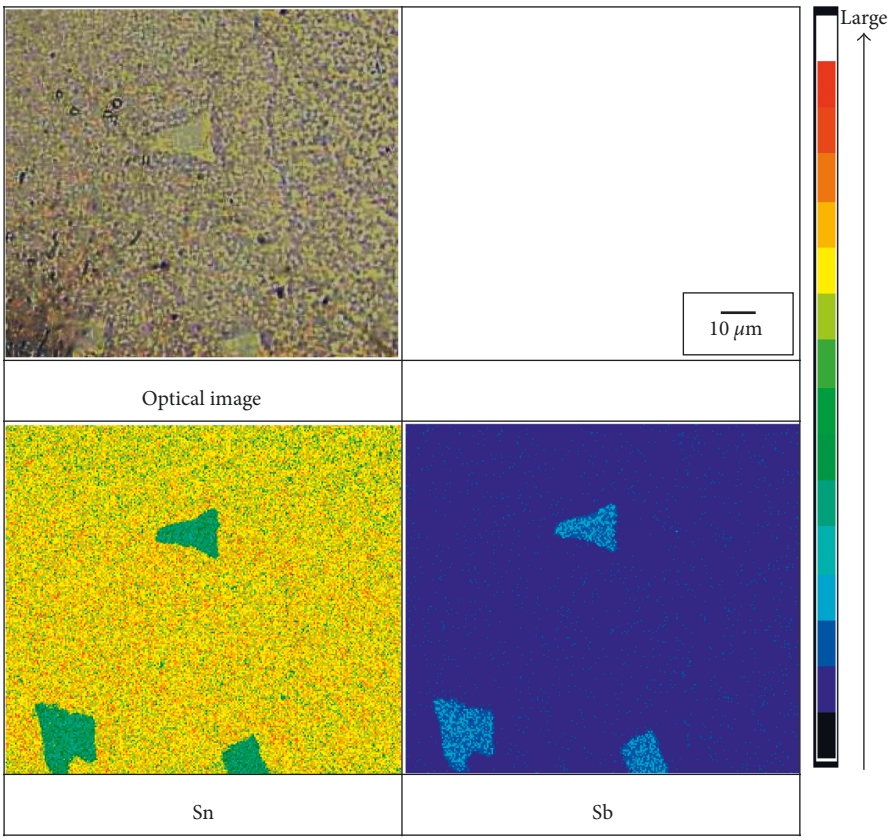


Figure 5: Laser scanning microscope image of Sn-10Sb and corresponding EPMA composition maps.

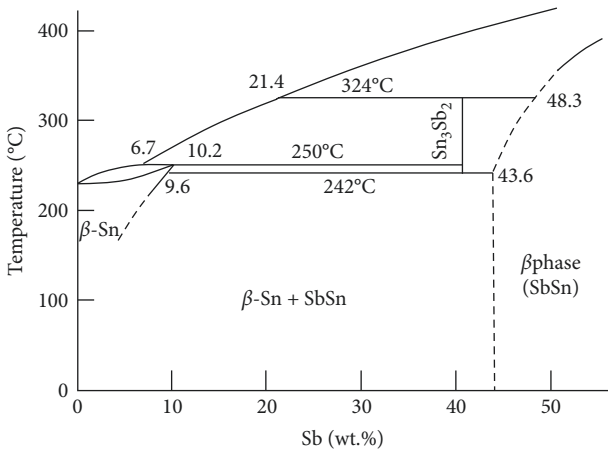


Figure 6: Sn-Sb binary phase diagram [17].

In both alloys, very fine dark-gray and bright-gray phases with submicrometer sizes were observed.

Figures 4 and 5 show optical images of as-cast miniature size specimens and the EPMA mapping analysis results of Sn-5Sb and Sn-10Sb, respectively.

Figure 6 shows the Sn-Sb binary phase diagram [17]. From the phase diagram, both Sn-5Sb and Sn-10Sb consist of $\beta$-Sn and SbSn phases. On the basis of the EPMA mapping analysis result and the Sn-Sb binary phase diagram, the dark-gray phase and the bright-gray phase, as shown in Figures 2 and 3, were inferred to be the $\beta$-Sn phase and the SbSn compound, respectively.

In Sn-10Sb, the distribution of 20~40 $\mu$m sizes of particles was observed in the optical image. From the EPMA mapping analysis result, the particles were inferred to be the SbSn compounds. Therefore, the formation of coarsened SbSn compounds occurs in the Sn-Sb alloy with increasing the Sb content.

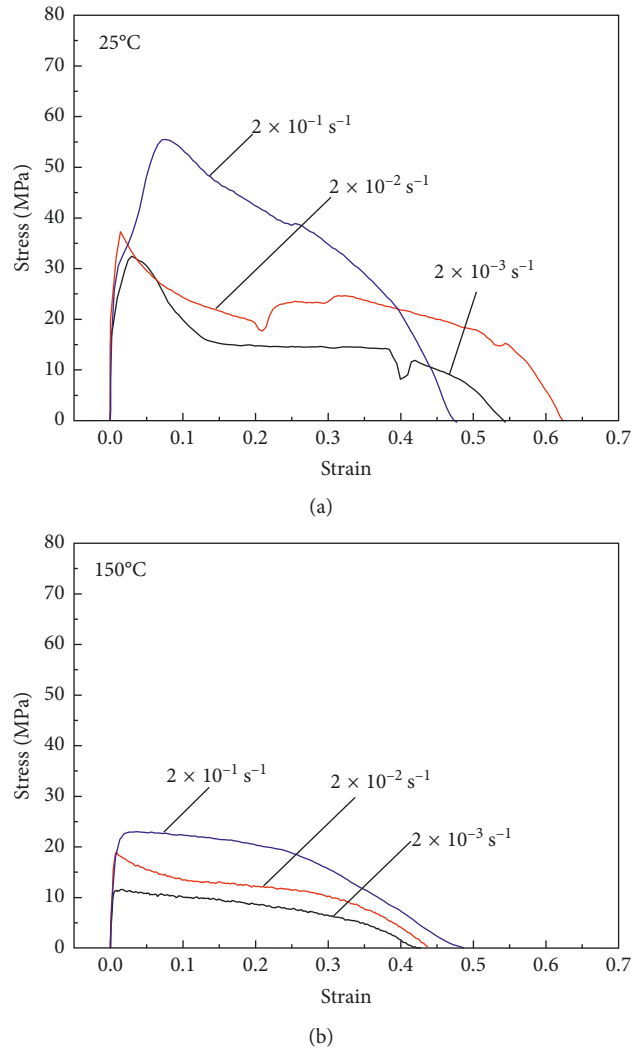


Figure 7: Typical stress-strain curves of Sn-5Sb [13]: (a) 25°C and (b) 150°C.

*3.2. Tensile Properties and Fracture Modes.* Figures 7 and 8 show typical stress-strain curves of miniature size specimens of Sn-5Sb and Sn-10Sb, respectively. Although the tensile strength of Sn-5Sb tends to increase with increasing the strain rate regardless of the test temperature, this tendency is not observed in Sn-10Sb at room temperature. Elongation of Sn-5Sb at 150°C and Sn-10Sb at both temperatures tends to increase with increasing the strain rate.

Figure 9 shows the effects of the strain rate and the test temperature on mechanical properties of Sn-5Sb [18] and Sn-10Sb alloys. Tensile strength and 0.1% proof stress of both alloys decrease with increasing the temperature. The tensile strength and 0.1% proof stress of Sn-10Sb are higher than those of Sn-5Sb at 25°C. It has been reported that the Berkovich hardness of the SbSn phase (approximately 1200 BHV) is four times that of the $\beta$-Sn (approximately 300 BHV) [19]. An increase of SbSn compounds in the Sn-Sb alloy with an increase of the Sb content results in increase of the tensile strength and 0.1% proof stress of the alloy. However, differences in them between both alloys are negligible at 150°C. From the binary Sn-Sb phase diagram, as shown in Figure 6, SbSn compounds decompose at high temperature so that the ratio of the SbSn compound decreases, and that of the $\beta$-Sn phase increases when the temperature rises to 150°C. Elongation of Sn-5Sb decreases with increasing the temperature except for a strain rate of $2 \times 10^{-1}$ s$^{-1}$, while that of Sn-10Sb increases with increasing the temperature. Elongation of Sn-5Sb is approximately 50% at the strain rate of $2 \times 10^{-1}$ s$^{-1}$, regardless of the temperature. Although elongation of Sn-10Sb is lower than that of Sn-5Sb at 25°C, the difference between them is small at 150°C.

Figures 10 and 11 show secondary electron images of Sn-5Sb and Sn-10Sb fractured specimens, respectively. In both alloys, chisel-point fracture was observed regardless of conditions of the tensile test. The tip of the break region was a straight line. It has been reported that a miniature size specimen consists of a few grains or a single grain so that the mechanical properties of the specimen strongly depend on the crystal orientation of the grain [15]. Since the slip systems of Sn that has tetragonal crystal structure are limited

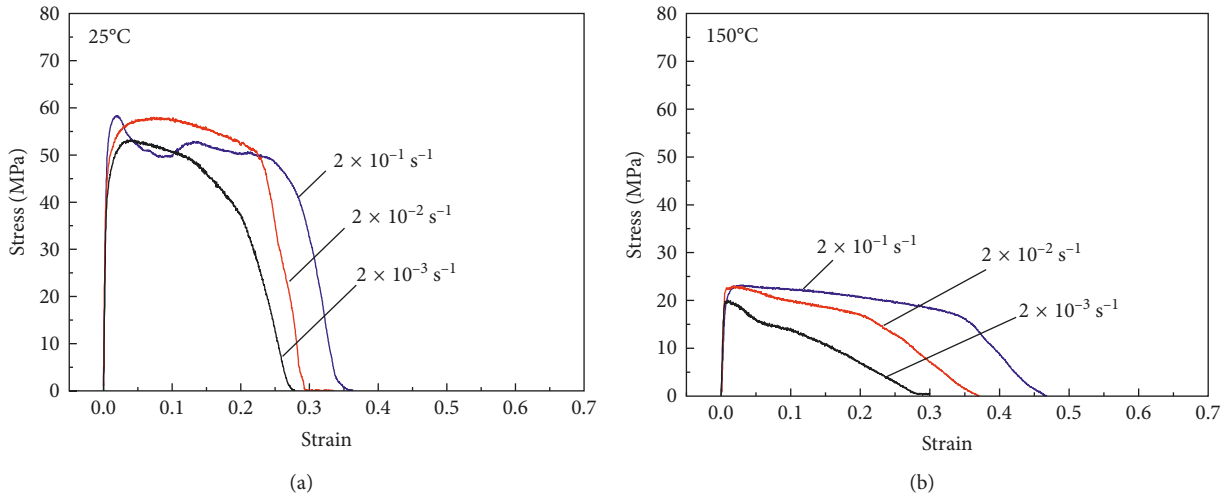


Figure 8: Typical stress-strain curves of Sn-10Sb: (a) 25°C and (b) 150°C.

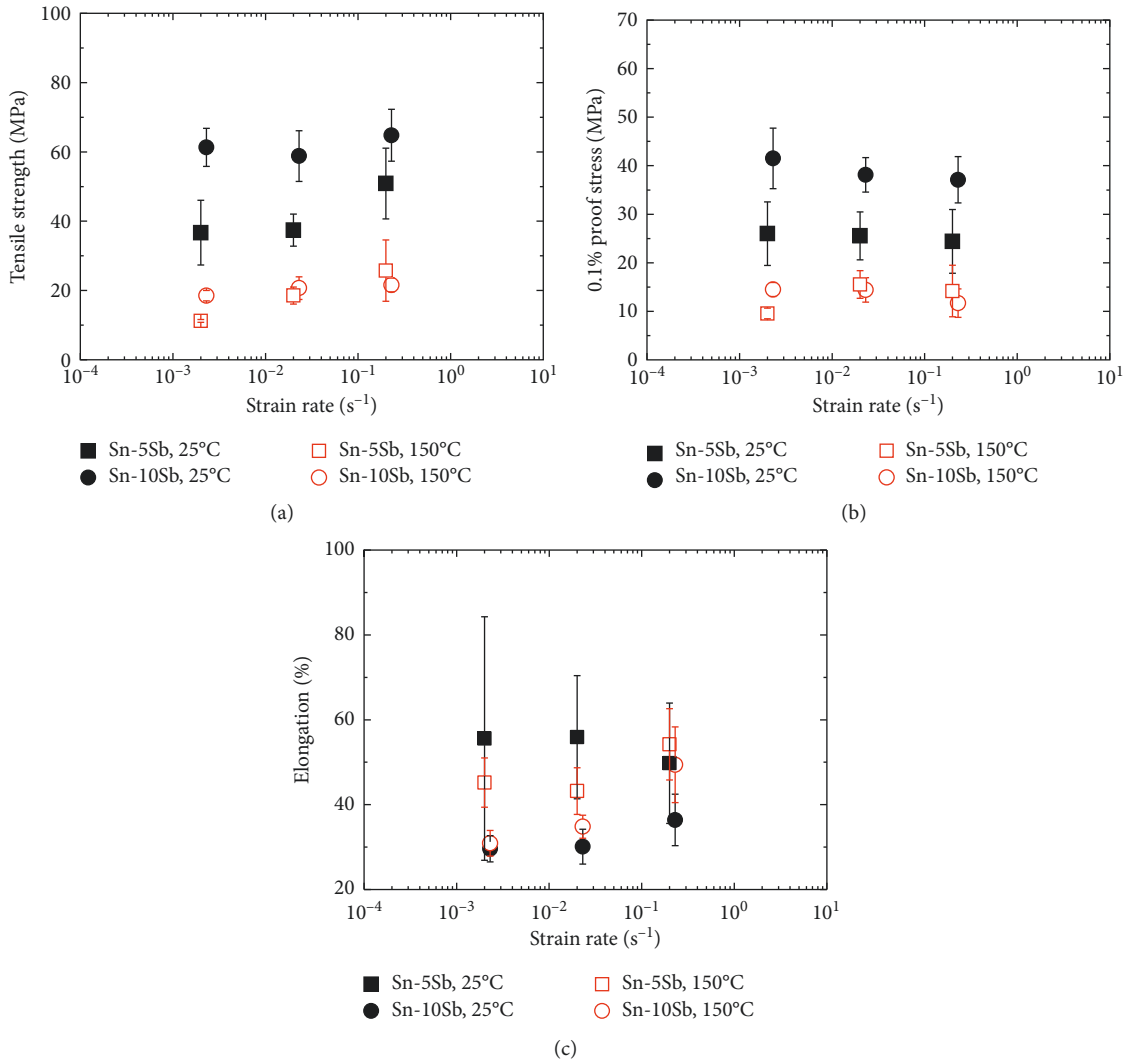


Figure 9: Comparison of mechanical properties of Sn-5Sb [18] and Sn-10Sb: (a) tensile strength, (b) 0.1% proof stress, and (c) elongation.

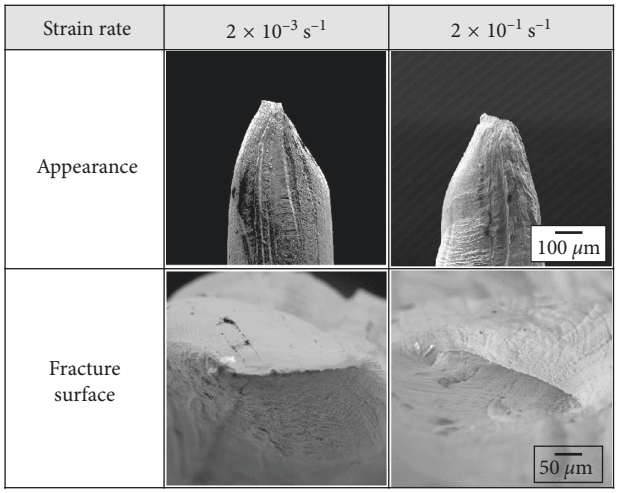


(a)

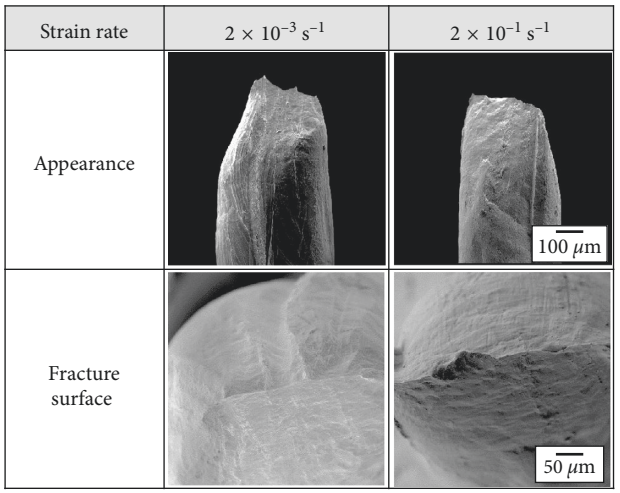


(b)

Figure 10: Secondary electron images of fractured specimens after tensile test of Sn-5Sb: (a) 25°C and (b) 150°C.

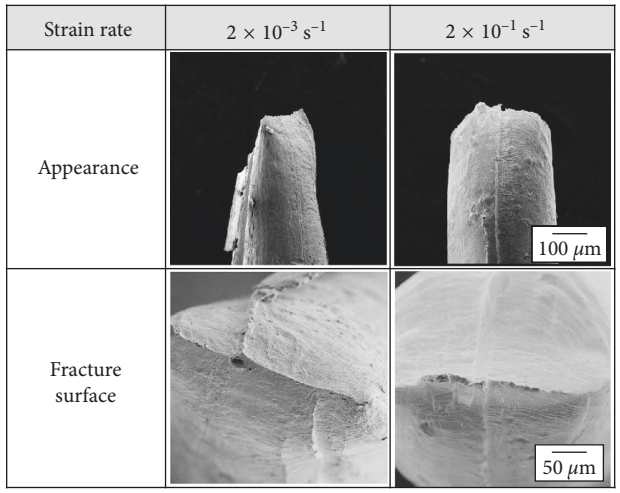


(a)

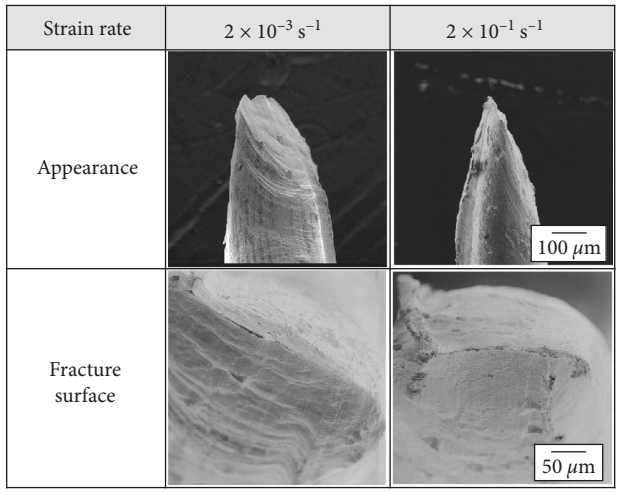


(b)

Figure 11: Secondary electron images of fractured specimens after tensile test of Sn-10Sb: (a) 25°C and (b) 150°C.

[20], the fractured area is not deformed uniformly, and thus, it is easily reduced in a straight line.

*3.3. Low Cycle Fatigue Properties and Fracture Modes.* Figure 12 shows the results of the low cycle fatigue tests with miniature size specimens of Sn-5Sb and Sn-10Sb, respectively. Typically, low cycle fatigue life of a solder alloy obeys the Manson–Coffin equation as follows:

$$\Delta\varepsilon_p = C_p \cdot N_f^{-\alpha}, \quad (1)$$

where $\Delta\varepsilon_p$ is plastic strain range, $C_p$ is fatigue ductility factor, $N_f$ is fatigue life, and $\alpha$ is fatigue ductility exponent.

From Figure 12, it was confirmed that low cycle fatigue lives of both alloys obey the Manson–Coffin equation, and fatigue ductility exponents, $\alpha$, are 0.54 for Sn-5Sb and 0.46 for Sn-10Sb, regardless of the temperature. In general, the isothermal fatigue life of a solder alloy degrades with increasing temperature [15]. However, Sn-Sb alloys exhibit no temperature dependence and have excellent isothermal fatigue properties in temperatures ranging from 25°C to 150°C.

Compared with Sn-5Sb and Sn-10Sb, $\alpha$ of Sn-10Sb was a little smaller than that of Sn-5Sb. This means that Sn-10Sb has superior fatigue properties compared with Sn-5Sb.

Figures 13 and 14 show fracture surfaces of specimens of Sn-5Sb and Sn-10Sb after the low cycle fatigue test. In Sn-5Sb, the fracture surface mostly formed with an angle of 45 degrees with respect to a tensile-compression axis direction regardless of strain rate and temperature. In Sn-10Sb, the fracture surface relatively becomes the shape with many irregularities. Table 1 shows the maximum height $R_z$ of the surface roughness of the Sn-5Sb and Sn-10Sb fracture surfaces. From this table, the surface roughness of the Sn-10Sb fracture surface was larger than that of Sn-5Sb. Figure 15 shows the cross-sectional microstructure of the fractured specimen of the Sn-10Sb alloy after the low cycle fatigue test. In the figure, coarse SbSn compounds are observed in the fracture surface area. Since SbSn compounds in the Sn-Sb alloy are hard to break, the crack progress turns

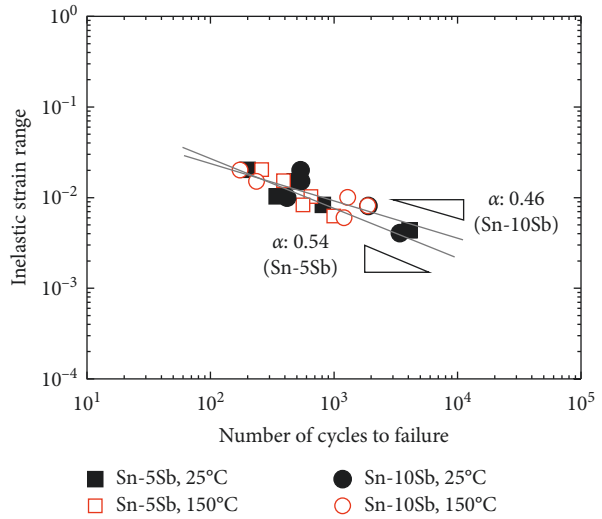


Figure 12: Low cycle fatigue properties of Sn-5Sb and Sn-10Sb.

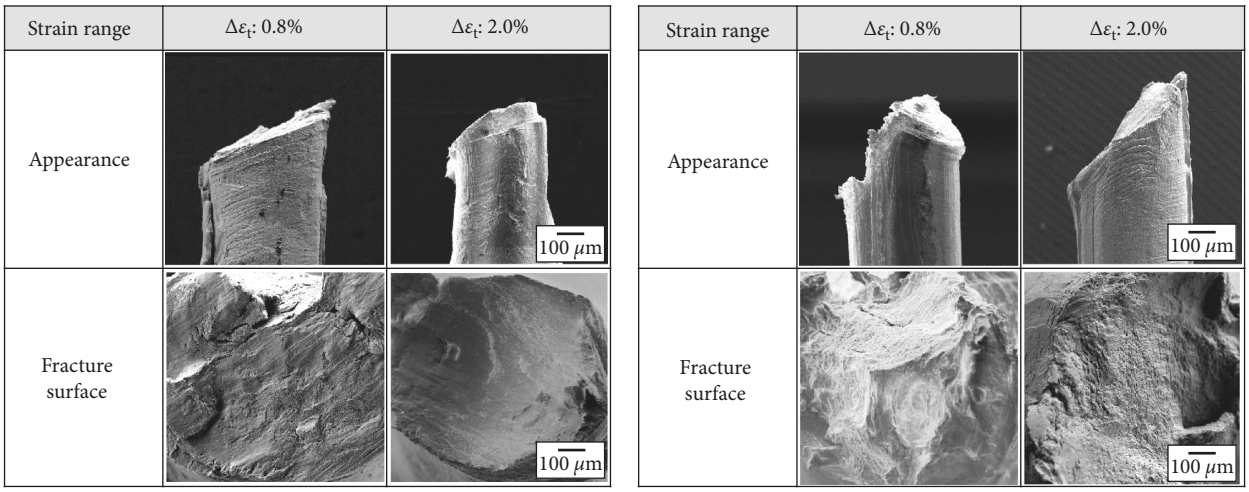


Figure 13: Secondary electron images of fracture specimens after low cycle fatigue test of Sn-5Sb: (a) 25°C and (b) 150°C.

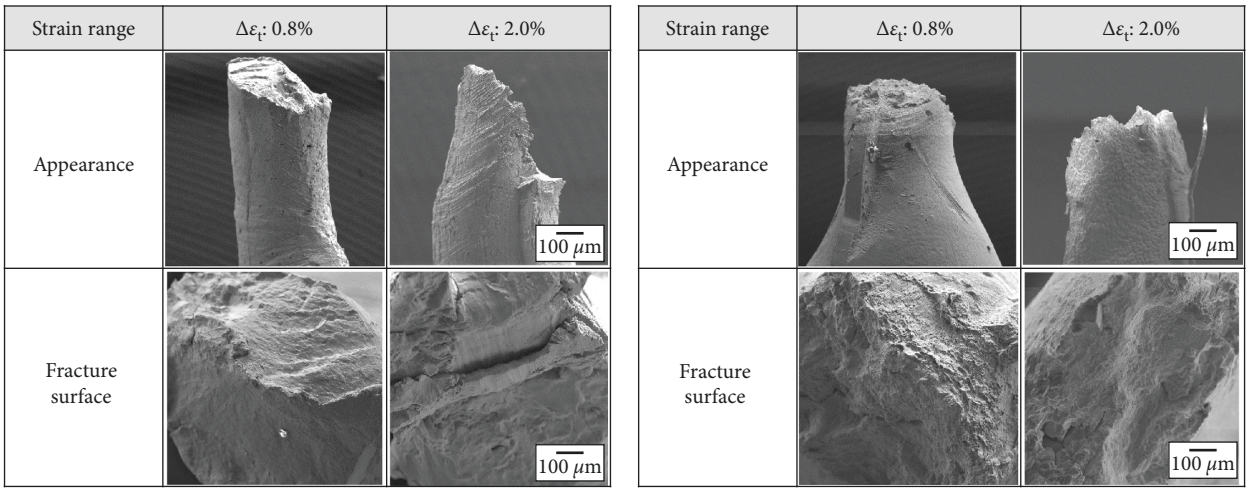


Figure 14: Secondary electron images of fracture specimens after low cycle fatigue test of Sn-10Sb: (a) 25°C and (b) 150°C.

Table 1: Obtained maximum height $R_z$.

| Solder type | Sn-5Sb | | | | Sn-10Sb | | | |
|---|---|---|---|---|---|---|---|---|
| Temperature (°C) | 25 | | 150 | | 25 | | 150 | |
| $\Delta\varepsilon_t$ (%) | 0.8 | 2.0 | 0.8 | 2.0 | 0.8 | 2.0 | 0.8 | 2.0 |
| $R_z$ ($\mu$m) | 26.5 | 33.5 | 93.5 | 48.4 | 105.2 | 125.6 | 162.6 | 102.9 |

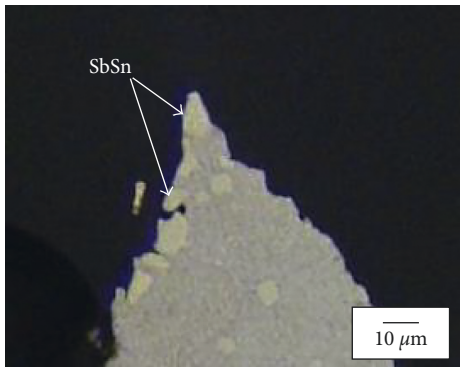


Figure 15: Optical image of cross-sectional microstructure of fractured specimen after low cycle fatigue test of Sn-10Sb (25°C, $\Delta\varepsilon_t$: 2.0%).

around the outer circumference of the SbSn compounds. Thus, the crack growth in Sn-10Sb, in which coarsened SbSn compounds occurred in as-cast microstructure (refer to Figure 5), is slower than that in Sn-5Sb, and the fracture surface of Sn-10Sb was very rough. As a result, it was clarified that the crack progress can be delayed by the formation of the coarse SbSn compounds in the Sn-Sb alloy, and thus, the fatigue properties can be improved.

## 4. Summary

In this study, tensile and fatigue properties of Sn-5Sb and Sn-10Sb alloys were compared using miniature size specimens. The results are listed as follows.

(1) $\beta$-Sn phases and SbSn compounds with submicrometer sizes were observed in Sn-5Sb, while the distribution of 20~40 $\mu$m size of SbSn compounds was also observed in Sn-10Sb.

(2) Tensile strength and 0.1% proof stress of both alloys decrease with increasing the temperature. The tensile strength and 0.1% proof stress of Sn-10Sb are higher than those of Sn-5Sb at 25°C, while differences in them between both alloys are negligible at 150°C. Elongation of Sn-5Sb decreases with increasing the temperature except for a strain rate of $2\times10^{-1}$ s$^{-1}$, while that of Sn-10Sb increases with increasing the temperature. Elongation of Sn-5Sb is approximately 50% at the strain rate of $2\times10^{-1}$ s$^{-1}$, regardless of the temperature. Although elongation of Sn-10Sb is lower than that of Sn-5Sb at 25°C, the difference between them is small at 150°C.

(3) The low cycle fatigue lives of Sn-5Sb and Sn-10Sb alloys obey the Manson–Coffin equation, and fatigue ductility exponents, $\alpha$, were 0.54 for Sn-5Sb and 0.46 for Sn-10Sb in the temperature range from 25°C to 150°C.

(4) On the basis of the observation of fractured specimens and the investigation of $\alpha$, it was clarified that the crack progress can be delayed by the formation of the coarse SbSn compounds in the Sn-Sb alloy, and thus the fatigue properties can be improved.

## Conflicts of Interest

The authors declare that they have no conflicts of interest.

## References

[1] V. Chidambaram, J. Hattel, and J. Hald, "High-temperature lead-free solder alternatives," *Microelectronic Engineering*, vol. 88, no. 6, pp. 981–989, 2011.

[2] K. Suganuma, S. J. Kim, and K. S. Kim, "High-temperature lead-free solders properties and possibilities," *JOM*, vol. 61, no. 1, pp. 64–71, 2009.

[3] T. Yamamoto and K. Tsubone, "Assembly technology using lead-free solder," *Fujitsu Scientific and Technical Journal*, vol. 43, no. 1, pp. 50–58, 2007.

[4] Z. Mei, H. A. Holder, and H. A. Vander Plas, "Low-temperature solders," *Hewlett-Packard Journal*, vol. 10, pp. 1–10, 1996.

[5] J. H. Kim, S. W. Jeong, and H. M. Lee, "Thermodynamics-aided alloy design and evaluation of Pb-free solders for high-temperature applications," *Materials Transactions*, vol. 43, no. 8, pp. 1873–1878, 2002.

[6] Y. Takaku, L. Felicia, I. Ohnuma, R. Kainuma, and K. Ishida, "Interfacial reaction between Cu substrates and Zn-Al base high-temperature Pb-free solders," *Journal of Electronic Materials*, vol. 37, no. 3, pp. 314–323, 2008.

[7] M. Nahavandi, M. A. Azmah Hanim, Z. N. Ismarrubie, A. Hajalilou, R. Rohaizuan, and M. Z. Shahrul Fadzli, "Effects of silver and antimony content in lead-free high-temperature solders of Bi-Ag and Bi-Sb on copper substrate," *Journal of Electronic Materials*, vol. 43, no. 2, pp. 579–585, 2014.

[8] Z. Haidong, I. Shohji, M. Shimoda, and H. Watanabe, "Effect of strain rate and temperature on tensile properties of Bi-based lead-free solder," *Materials Transactions*, vol. 57, no. 6, pp. 873–880, 2016.

[9] Y. T. Chen and C. C. Chen, "Interfacial reactions in Sn–Sb/Ni couples," *Journal of the Taiwan Institute of Chemical Engineers*, vol. 43, no. 2, pp. 295–300, 2012.

[10] S. Chen, A. Zi, P. Chen, H. Wu, Y. Chen, and C. Wang, "Interfacial reactions in the Sn–Sb/Ag and Sn–Sb/Cu couples," *Materials Chemistry and Physics*, vol. 111, no. 1, pp. 17–19, 2008.

[11] S. W. Chen, C. C. Chen, W. Gierlotka, A. R. Zi, P. Y. Chen, and H. J. Wu, "Phase equilibria of the Sn-Sb binary system," *Journal of Electronic Materials*, vol. 37, no. 7, pp. 992–1002, 2008.

[12] K. Kobayashi, I. Shohji, and H. Hokazono, "Tensile and fatigue properties of miniature size specimens of Sn-5Sb lead free solder," *Materials Science Forum*, vol. 879, pp. 2377–2382, 2016.

[13] K. Kobayashi, I. Shohji, S. Koyama, and H. Hokazono, "Fracture behaviors of miniature size specimens of Sn-5Sb lead-free solder under tensile and fatigue conditions," *Procedia Engineering*, vol. 184, pp. 238–245, 2017.

[14] A. Morozumi, H. Hokazono, Y. Nishimura, E. Mochizuki, and Y. Takahashi, "Influence of antimony on reliability of solder joints using Sn-Sb binary alloy for power semiconductor modules," *Transactions of the Japan Institute of Electronics Packaging*, vol. 8, no. 1, pp. 8–17, 2015.

[15] Y. Kariya, T. Niimi, T. Suga, and M. Otsuka, "Isothermal fatigue properties of Sn-Ag-Cu alloy evaluated by micro size specimen," *Materials Transactions*, vol. 46, no. 11, pp. 2309–2315, 2005.

[16] I. Shohji, T. Osawa, T. Matsuki, Y. Kariya, K. Yasuda, and T. Takemoto, "Effect of specimen size and aging on tensile properties of Sn-Ag-Cu lead-free solders," *Materials Transactions*, vol. 49, no. 5, pp. 1175–1179, 2008.

[17] T. B. Massalski, *Binary Alloy Phase Diagrams*, ASM International, New York, NY, USA, 1990.

[18] T. Kobayashi, M. Yokoi, K. Kobayashi, K. Mitsui, and I. Shohji, "Comparison of Sn-Sb and Sn-Ag-Cu-Ni-Ge alloys using tensile properties of miniture size specimens," *Solid State Phenomena*, vol. 273, pp. 83–90, 2018.

[19] Y. Toyama and I. Shohji, "Effect of strain rate on tensile properties of miniature size lead-free alloys," in *Proceedings of the 35th IEEE/CPMT International Electronics Manufacturing Technology Conference (IEMT)*, Ipoh, Malaysia, November 2012.

[20] A. U. Telang and T. R. Bieler, "The orientation imaging microscopy of lead-free Sn-Ag solder joints," *JOM*, vol. 57, no. 6, pp. 44–49, 2005.